A novel fast phase correlation algorithm for peak wavelength detection of fiber Bragg gratings sensors

Lamberti, Alfredo; Vanlanduit, Steve; De Pauw, Ben; Berghmans, Francis

Published in:
Opt. Express

Publication date:
2014

Document Version:
Final published version

A novel fast phase correlation algorithm for peak wavelength detection of fiber Bragg grating sensors

A. Lamberti,[1,*] **S. Vanlanduit,**[1] **B. De Pauw,**[1,2] **and F. Berghmans**[2]

[1]*Department of Mechanical Engineering Vrije Universiteit Brussel, Pleinlaan 2, 1050 Elsene, Belgium*

[2]*Department of Applied Physics and Photonics Vrije Universiteit Brussel, Pleinlaan 2, 1050 Elsene, Belgium*

[*]*allamber@vub.ac.be*

Abstract: Fiber Bragg Gratings (FBGs) can be used as sensors for strain, temperature and pressure measurements. For this purpose, the ability to determine the Bragg peak wavelength with adequate wavelength resolution and accuracy is essential. However, conventional peak detection techniques, such as the maximum detection algorithm, can yield inaccurate and imprecise results, especially when the Signal to Noise Ratio (SNR) and the wavelength resolution are poor. Other techniques, such as the cross-correlation demodulation algorithm are more precise and accurate but require a considerable higher computational effort. To overcome these problems, we developed a novel fast phase correlation (FPC) peak detection algorithm, which computes the wavelength shift in the reflected spectrum of a FBG sensor. This paper analyzes the performance of the FPC algorithm for different values of the SNR and wavelength resolution. Using simulations and experiments, we compared the FPC with the maximum detection and cross-correlation algorithms. The FPC method demonstrated a detection precision and accuracy comparable with those of cross-correlation demodulation and considerably higher than those obtained with the maximum detection technique. Additionally, FPC showed to be about 50 times faster than the cross-correlation. It is therefore a promising tool for future implementation in real-time systems or in embedded hardware intended for FBG sensor interrogation.

OCIS codes: (060.2370) Fiber optics sensors; (050.2770) Gratings; (070.4790) Spectrum analysis; (070.7145) Ultrafast processing.

References and links

1. K.O. Hill, Y. Fujii, D. C. Johnsen, and B. S. Kawasaki, "Photosensitivity in optical fiber waveguides: Application to reflection filter fabrication," Appl. Phys. Lett. **32**, 647–649 (1978).
2. G. Meltz, W. W. Morey, and W. H. Glenn, "Formation of Bragg gratings in optical fibers by a transverse holographic method," Opt. Lett. **14**, 823–825 (1989).
3. K. O. Hill and G. Meltz, "Fiber Bragg grating technology fundamentals and overview," J. Lightwave Technol. **15**(8), 1263–1276 (1997).
4. A. D. Kersey, M. A. Davis, H. J. Patrick, M. LeBlanc, K. P. Koo, C. G. Askins, M. A. Putnam, and E. J. Friebele, "Fiber grating sensors," J. Lightwave Technol. **15**(8), 1442–1463 (1997).
5. Y. Yu, H. Tam, W. Chung, and M. S. Demokan, "Fiber Bragg grating sensor for simultaneous measurements of displacement and temperature," Opt. Lett. **25**(16), 1141–1143 (2000).

#202834 - $15.00 USD Received 11 Dec 2013; revised 12 Feb 2014; accepted 16 Feb 2014; published 19 Mar 2014

6. X. Shu, Y. Liu, D. Zhao, B. Gwandu, F. Floreani, L. Zhang, and I. Bennion, "Dependence of temperature and strain coefficients on fiber grating type and its application to simultaneous temperature and strain measurement," Opt. Lett. **27**(9), 701–703 (2002).
7. S. Melle, K. Liu, and R. M. Measures, "A passive wavelength demodulation system for guided-wave Bragg grating sensors," IEEE Photonics Technol. Lett. **4**(5), 516–518 (1992).
8. G. A. Ball, W. W. Morey, and R. K. Cheo, "Fiber laser source/analyzer for Bragg grating sensor array interrogation," J. Lightwave Technol. **12**(4), 700–703 (1994).
9. R. Huber, D. C. Adler, and J. G. Fujimoto, "Buffered Fourier domain mode locking: unidirectional swept laser sources for optical coherence tomography imaging at 370,000 lines/s," Opt. Lett. **31**(20), 2975–2977 (2006).
10. C. G. Atkins, M. A. Putnam, and E. J. Friebele, "Instrumentation for interrogating many-element fiber Bragg grating arrays," Proc. SPIE **2444**, 257–267 (1995).
11. A. Ezbiri, S. E. Kanellopoulos, and V. A. Handerek, "High resolution instrumentation system for fiber-Bragg grating aerospace sensors," Opt. Commun. **150**, 43–48 (1998).
12. J. M. Gong, J. M. K. MacAlpine, C. C. Chan, W. Jin, M. Zhang, and Y. B. Liao, "A novel wavelength detection technique for fiber Bragg grating sensors," IEEE Photonics Technol. Lett. **14**(5), 678–680 (2002).
13. C. Caucheteur, K. Chah, F. Lhommé, M. Blondel, and P. Mégret, "Autocorrelation demodulation technique for fiber Bragg grating sensor," IEEE Photonics Technol. Lett. **16**(10), 2320–2322 (2004).
14. C. Huang, W. Jing, K. Liu, Y. Zhang, and G. D. Peng "Demodulation of fiber Bragg grating sensor using cross-correlation algorithm," IEEE Photonics Technol. Lett. **19**(9), 707–709 (2007).
15. L. Negri, A. Nied, H. Kalinowsky, and A. Paterno "Benchmark of peak detection algorithms in fiber Bragg grating interrogation and a new neural network for its performance improvement," Sensors **11**, 3466–3482 (2011).
16. L. Gui and S. T. Wereley, "A correlation-based continuous window-shift technique to reduce the peak-locking in digital PIV evaluation," Experiments Fluids **32**, 506–517 (2002).
17. A. C. Eckstein and J. Charonko "Phase correlation processing for DPIV measurements," Experiments Fluids **45**, 485–500 (2008).
18. M. Raffel, C. Willert, and J. Kompenhans, *Particle Image Velocimetry—A Practical Guide* (Springer, 1998).
19. K. T. Christensen, "On the influence of peak-locking errors on turbulance statistics compared from piv ensembles," Experiments Fluids **36**(3), 484–497 (2004).
20. J. Westerweel, "Fundamentals of digital particle image velocimetry," Meas. Sci. Technol. **8**(12), 1379–1392 (1997).
21. R. Kashyap, *Fiber Bragg Gratings* (Academic, 1999), Vol. IV.
22. H. Y. Ling, K. T. Lau,W. Jin, and K. C. Chan, "Characterization of dynamic strain measurement using reflection spectrum from a fiber Bragg grating," Opt. Commun. **270**, 25–30 (2007).
23. Y. J. Rao, "In-fibre Bragg grating sensors," Meas. Sci. Technol. **8**, 355–377 (1997).
24. Optical Sensing Interrogator sm125, http://micronoptics.com/uploads/library/documents/datasheets/instruments.

1. Introduction

Fiber Bragg gratings (FBGs) made their first appearance about 30 years ago [1, 2]. Their common characteristics, such as small size, low weight, insensitivity to electromagnetic interference, chemical inertness, high durability and resistance to corrosion, have made them extremely attractive for the engineering community. FBGs are now widely used for sensing applications [3–6] in the aerospace, automotive, petrochemical and biomedical industry. The working principle of a FBG sensor is based on the shift of the Bragg wavelength occurring when the FBG is subjected to physical parameters such as strain, stress, vibrations, temperature and pressure. Accurately measuring these physical parameters therefore requires an accurate measurement of the Bragg wavelength shift. Many demodulation schemes for FBG wavelength shift monitoring have been developed, based for example on optical edge filters [7], on tunable fiber laser sources [8], and on Fourier domain mode locking-technology [9]. These interrogation techniques have reached a wavelength scanning frequency of several thousands of Hz [9], necessitating high speed acquisition and computation capabilities. One way to speed up the acquisition process is to reduce the amount of samples and hence the wavelength resolution. However, conventional peak detection (CPD) techniques proposed in literature, such as the maximum detection algorithm (MDA), the centroid detection algorithm (CDA) [10] and the polynomial fitting algorithm, often produce poor results for low sample spectral resolution. Moreover CPD techniques are very sensitive to noise. On the other hand, they are reasonably fast and easy to implement. More recently implemented peak detection techniques, such as the least squares (LSQ) [11]

#202834 - $15.00 USD Received 11 Dec 2013; revised 12 Feb 2014; accepted 16 Feb 2014; published 19 Mar 2014

algorithm, the minimum variance shift (MVS) [12] technique, the auto-and cross-correlation algorithms (ACA, CCA) [13, 14], and the artificial neural network method [15], produce better results and are less affected by wavelength resolution and noise. In particular, the CCA algorithm demonstrated to achieve the most precise results while the neural network algorithm showed to be less sensitive to distortion of the FBG spectrum. However, a major drawback of these algorithms is the computation time, which is considerably higher compared to CPD techniques and might not meet the requirements of many dynamic sensing systems. A further problem common to all peak detection techniques is the so called peak locking effect. This phenomenon has been widely studied in the particle-image velocimetry (PIV) community [16, 17] but, to the best of our knowledge, it has never been considered in FBG applications up to now. It consists in a modulation of both precision and accuracy errors, with minimum errors occurring at integer resolution positions, and maximum errors biased toward mid-resolution positions. Peak locking depends mainly on wavelength resolution and on the choice of the sub-resolution estimator. [18, 19]. For example, with a wavelength resolution of 1 pm, in the case of a true wavelength shift of 10.4 pm, the sub-interpolation estimator will lock the estimated wavelength closer to 10 pm. On the other hand, a true wavelength of 10.6 pm would be estimated closer to 11 pm. Therefore, because of the peak locking error, true wavelength shifts that exist between integer wavelength positions are inevitably pushed towards the nearest integer wavelength position, with a consequent degradation of both accuracy and precision. This behavior is further influenced by the type of sub-interpolation estimator used. For instance, for PIV applications, it has been demonstrated that Gaussian interpolation performs better than both centroid and quadratic fits in terms of mitigating peak-locking effects [20]. All these considerations need to be take into account in the evaluation of the performance of any peak detection algorithm if misinterpretation of data wants to be avoided.

In this paper, we propose a fast and accurate peak detection algorithm based on fast phase-correlation (FPC). The FPC algorithm determines the wavelength shift from the phase shift between the undisturbed FBG spectrum and the perturbed spectrum. Using simulations, we investigated the effects of sample resolution, peak locking and SNR on the precision and accuracy of the FPC algorithm. At the same time, we compared the obtained FPC performance with those of two other algorithms: the MDA algorithm with an integrating 10 points quadratic interpolation routine and the CCA algorithm with a 3rd order polynomial subpixel interpolation. The FPC precision and accuracy were of the same order of those obtained with the CCA and considerably better than those provided by the MDA. However, the FPC showed a more attenuated peak locking effect than MDA and CCA. At the same time, the computation time of the FPC was up to 50 times lower than the time required by the CCA. Experiments were carried out to validate the simulations. A cylindrical steel beam with three FBGs glued on its lateral surface was axially loaded with a tensile test machine. The measurements confirmed the effectiveness of the FPC algorithm.

Our paper is further structured as follows, In Section 2 we introduce the principles of the fast phase-correlation method. Section 3 deals with our simulation results, for which we compared the performance of different algorithms on simulated Bragg grating spectra. Section 4 summarizes the experimental results and compares how the different peak detection methods behave when applied to experimentally obtained Bragg grating responses. To close, Section 5 concludes on the performances of our proposed FPC algorithm for different wavelength resolutions and SNR levels.

2. Fast Phase Correlation (FPC) working principle

FBG based sensing relies on tracking the Bragg peak wavelength as it shifts with a change in the measurand. In the proposed FPC algorithm, we start from a reference FBG reflec-

#202834 - $15.00 USD Received 11 Dec 2013; revised 12 Feb 2014; accepted 16 Feb 2014; published 19 Mar 2014

tion spectrum. This reference spectrum does not necessarily have to correspond to the undisturbed spectrum, which is the spectrum before the measurand acts on the FBG. The reference spectrum is recorded as $R(\lambda_j)$, where λ_j represents the j^{th} element of the wavelength vector and j=1,2,...,(N-1). The number of samplings N depends on the wavelength scanning range $\lambda_{max} - \lambda_{min}$ and on the wavelength resolution $\delta\lambda$.

$$N = \frac{\lambda_{max} - \lambda_{min}}{\delta\lambda} \tag{1}$$

When the measurand acts on the FBG, the perturbed spectrum is stored in a second vector $R'(\lambda_j)$, for j=1,2,...,(N-1). Assuming that there is no distortion of the spectrum, the perturbed spectrum $R'(\lambda_j)$ can be rewritten as

$$R'(\lambda_j) = R(\lambda_j - \Delta\lambda) \tag{2}$$

where $\Delta\lambda$ is the wavelength shift between R and R'. In order to evaluate $\Delta\lambda$, the FPC algorithm first computes the fast Fourier trasforms $\Re(k)$ and $\Re'(k)$ of $R(\lambda_j)$ and $R'(\lambda_j)$ respectively

$$\Re(k) = \sum_{j=1}^{N-1} R(\lambda_j)\, e^{\frac{-2\pi i}{N}(j-1)(k-1)}, \quad k = 1,2,\ldots,M << N \tag{3}$$

$$\Re'(k) = \sum_{j=1}^{N-1} R'(\lambda_j)\, e^{\frac{-2\pi i}{N}(j-1)(k-1)}, \quad k = 1,2,\ldots,M << N \tag{4}$$

with k indicating the generic Fourier spectral line and M the maximum number of spectral lines considered in the analysis.
For each value of k, starting from k = 2 to $k = M$, an estimation $\hat{\Delta\lambda}$ of the wavelength shift is calculated in the following way:

$$\hat{\Delta\lambda}(k-1) = \left(\angle\Re'(k) - \angle\Re(k)\right)\frac{Nk\,\delta\lambda}{2\pi}, \quad k = 2,\ldots,M << N \tag{5}$$

where the symbol $\angle$ indicates the phase of the complex number. The wavelength shift $\Delta\lambda$ is then obtained taking the median value of the previously computed estimates

$$\Delta\lambda = \underset{2\le k\le M}{\text{median}}\left(\hat{\Delta\lambda}(k-1)\right) \tag{6}$$

The choice of the median instead of other metrics, such as the mean, stems from considering the robustness of the computation: the median is less sensitive to outliers. It must be noted that one normally chooses M=N. In this case, however, M can be set to be considerably lower than N, since only the first few frequency lines of R and R' contain energy. Such an energy distribution is due to the shape of both spectra R and R', which can be approximated by "sinc" functions. If the main lobe width of these sinc functions is indicated by r_B, then the Fourier transforms $\Re$ and $\Re'$ result to be rectangular-shaped, with energy distributed only within the frequency band 0-$r_B/2$. Therefore, the narrower is the peak, the lower is the number of spectral lines M required for the analysis. When $M << N$, as in Eqs. (3)–(4), the FPC algorithm avoids to compute $(N-M) \times N$ terms for each of the FFT in Eqs. (3)–(4), with a consequent advantage in terms of execution speed.

3. Simulation and results

To evaluate the FPC algorithm introduced above, we first developed a Matlab script to simulate the dynamic behavior of an FBG subjected to a given deformation field. Then, we processed the

#202834 - $15.00 USD Received 11 Dec 2013; revised 12 Feb 2014; accepted 16 Feb 2014; published 19 Mar 2014

simulated data using both the FPC and two other algorithms, the maximum detection algorithm (MDA) and the cross-correlation demodulation (CCA) algorithm. The MDA algorithm includes a 10 points quadratic interpolation around the maximum position, while the CCA script also integrates a subpixel polynomial interpolation routine. Finally, we compared the performances of the three algorithms in terms of precision, accuracy and computation time. Section 3.1 describes the principle of the dynamic FBG simulation, while section 3.2 explains the processing procedure of the simulated FBG spectra and reports on the performances obtained for different SNR values and wavelength resolutions.

3.1. Simulation of FBG under dynamical strain.

According to the Couple-Mode theory, the mode propagation through the grating of an FBG is described by the following system of first order differential equations [21]

$$\frac{dR(z)}{dz} = i\left(k_{dc}R(z) + k_{ac}S(z)\right) \tag{7}$$

$$\frac{dS(z)}{dz} = -i\left(k_{dc}S(z) + k_{ac}R(z)\right) \tag{8}$$

where z is the mode direction of propagation, $R(z)$ and $S(z)$ are the amplitudes of the forward- and backward-propagating modes. k_{dc} and k_{ac} are respectively the "dc" and "ac" self-coupling coefficients. For a uniform grating k_{dc} and k_{ac} can be expressed as [21, 22]:

$$k_{dc} = 2\pi n_{\text{eff}}\left(\frac{1}{\lambda} - \frac{1}{\lambda_D}\right) + \frac{2\pi}{\lambda}\overline{\delta n_{\text{eff}}} \tag{9}$$

$$k_{ac} = \frac{\pi}{\lambda}\,\nu\,\overline{\delta n_{\text{eff}}} \tag{10}$$

where n_{eff} is the effective index modulation, $\overline{\delta n_{\text{eff}}}$ is the "dc" index change spatially averaged over a grating period Λ_0, $\lambda_D = 2n_{\text{eff}}\Lambda_0$ is the designed Bragg wavelength and ν is the fringe visibility. Assuming that the length of the grating is L, the reflecivity is given by

$$R(\lambda) = \left|\frac{S(-L/2)}{R(-L/2)}\right|^2. \tag{11}$$

Using the T-matrix formulation Eq. (11) can be computed as follows:

$$\begin{bmatrix} R(-L/2) \\ S(-L/2) \end{bmatrix} = \prod_{r=1}^{m} T_r \times \begin{bmatrix} R(L/2) \\ S(L/2) \end{bmatrix} \tag{12}$$

where m is the number of sections in which the grating is divided and T_r is the r^{th} transfer matrix

$$T_r = \begin{bmatrix} \cosh(\alpha\Delta z) - i\frac{k_{dc}}{\alpha}\sinh(\alpha\Delta z) & -i\frac{k_{ac}}{\alpha}\sinh(\alpha\Delta z) \\ i\frac{k_{ac}}{\alpha}\sinh(\alpha\Delta z) & \cosh(\alpha\Delta z) - i\frac{k_{dc}}{\alpha}\sinh(\alpha\Delta z) \end{bmatrix} \tag{13}$$

$$\alpha = \sqrt{{k_{ac}}^2 - {k_{dc}}^2} \tag{14}$$

In order to simulate the dynamical behavior of the FBG, the following strain function along the z axis is assumed

$$\varepsilon_{zz}(z,t) = C_0 t \tag{15}$$

#202834 - $15.00 USD Received 11 Dec 2013; revised 12 Feb 2014; accepted 16 Feb 2014; published 19 Mar 2014

where C_0 is a constant. In this circumstance, the design wavelength λ_D in (9) becomes

$$\lambda_D(z,t) = 2n_{\text{eff}}\Lambda_0\left(1 + a\varepsilon(z,t)\right) \tag{16}$$

where $a = 1 - \frac{1}{2}n_{\text{eff}}\left[p_{12} - \upsilon\left(p_{11} - p_{12}\right)\right]$ is the grating gauge factor [22, 23], in which p_{11} and p_{12} are the components of the fibre-optic strain tensor and υ is the Poisson's ratio. At each time step, the developed Matlab script recalculates the value of λ_D and refreshes the value of k_{dc} needed for the computation of the reflectivity according to Eq. (11). This numerical procedure was used to simulate the behavior of an FBG with $L = 10^{-2}$ m, $\Lambda_0 = 10^{-7}$ m, $n_{\text{eff}} = 1.452$, $\overline{\delta n_{\text{eff}}} = 1.131 \times 10^{-4}$, $\nu = 1$, $p_{11} = 0.121$, $p_{12} = 0.270$, $\upsilon = 0.17$. The Bragg wavelength of the grating in a strain-free state is 1540.16 nm. The normalized reflectivity was computed for a uniform strain of $C_0 = 10^{-4}\ \mu\varepsilon$. Figure 1 shows the normalized reflectivity and the wavelength shift $\Delta\lambda_D$ as a function of time.

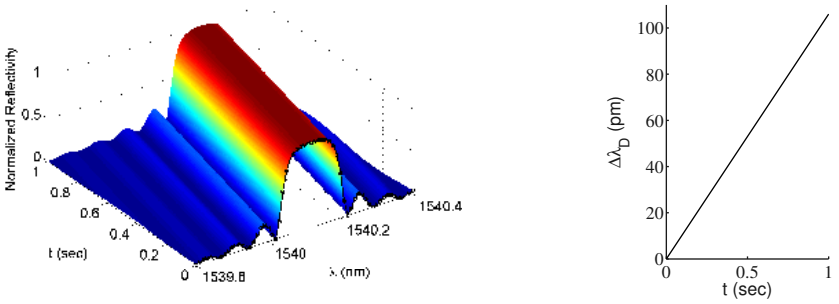

(a) (b)

Fig. 1. (a) Normalized reflectivity against wavelength and time under a uniform constant strain $C_0 = 10^{-4}\ \mu\varepsilon$. The black line with markers indicates the strain-free spectrum. (b) Theoretical shift of the design wavelength.

It is worth noting that for unchirped gratings subjected to uniform axial strain $\varepsilon(z)$, the reflectivity can be directly calculated from the exact solution. However, the transfer matrix-method was hier used in order to implement a procedure capable to perform the analysis on any kind of grating subjected to any kind of axial strain. In future works a similar procedure will be used to simulate and analize the behavior of FBG under dynamical non uniform strain fields.

3.2. Processing of simulated FBG spectra and performance analysis.

The FBG spectra simulated in Section 3.1 were used to test the FPC algorithm presented in section 2. The strain-free spectrum was chosen as the reference spectrum $R(k)$ while the reflectivity at each time instant was taken as the vector $R'(k)$. To simulate signals with different signal-to-noise ratios, white Gaussian noise (AWGN) was added to the instantaneous reflectivity. Signals were generated for SNR values of 30 dB up to 60 dB in steps of 5 dB. For each SNR level, the wavelength shift was computed 500 times to determine the statistics of the peak detection error. Figure 2 provides a graphical explanation of the procedure.

The precision σ_{SNR} and accuracy δ_{SNR} of the FPC algorithm for each SNR were computed according with the following definitions:

#202834 - $15.00 USD Received 11 Dec 2013; revised 12 Feb 2014; accepted 16 Feb 2014; published 19 Mar 2014

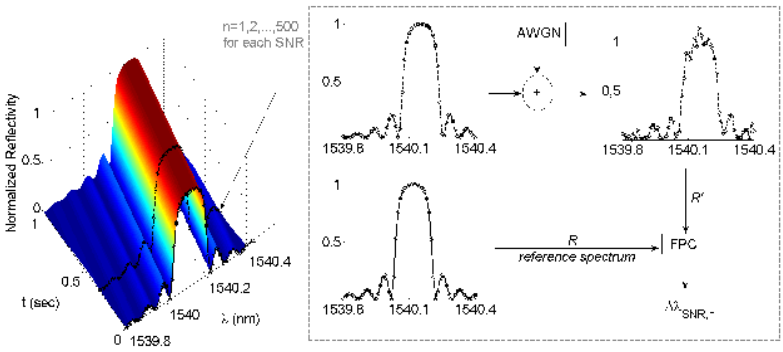

Fig. 2. Processing of the simulated spectra. The $R(k)$ and $R'(k)$ vectors are the input for the FPC algorithm which computes the wavelength shift 500 times for each SNR level.

$$\sigma_{SNR} = \sqrt{\frac{1}{500}\sum_{n=1}^{500}\left[(\Delta\lambda_{SNR,n} - \Delta\lambda_D) - \frac{1}{500}\sum_{n=1}^{500}(\Delta\lambda_{SNR,n} - \Delta\lambda_D)\right]^2} \tag{17}$$

$$\delta_{SNR} = \frac{1}{500}\sum_{n=1}^{500}|\Delta\lambda_{SNR,n} - \Delta\lambda_D| \tag{18}$$

where $\Delta\lambda_{SNR,n}$ is the calculated wavelength shift for the given SNR at the n^{th} repetition and $\Delta\lambda_D$ is the corresponding shift of the design wavelength obtained from Eq. (16). It is worth to notice that lower values of σ and δ indicate better precision and accuracy.
Figures 3 and 4 show the computed precision and accuracy of the FPC algorithm in comparison with the MDA and CCA peak detection techniques.

The maximum number of spectral lines used in the FPC algorithm is M=7. Four different sample resolutions $\delta\lambda$ were considered: 10 pm (Figs. 3(a) and 4(a)), 25 pm (Figs. 3(b) and 4(b)), 30 pm (Figs. 3(c) and 4(c)) and 35 pm (Figs. 3(d) and 4(d)). The results show that, although both FPC and CCA perform generally better than the MDA, the comparison of both precision and accuracy changes from one wavelength shift $\Delta\lambda$ to another. This is due to the peak locking effect, which is low for high resolution ($\delta\lambda$=10 pm) but becomes dominant as the resolution decreases ($\delta\lambda$=35 pm). Because of peak locking, an algorithm could be erroneously considered more or less precise and accurate than another. For example, looking at Figs. 3(c) and 4(c), at SNR=60 dB and $\Delta\lambda$=7 pm, the precision of FPC, CCA and MDA are respectively 0.14 pm, 0.09 pm and 0.77 pm. So one would conclude that the FPC precision improves by 82% compared to MDA but decreases by 35% compared to CCA. In terms of accuracy, for the same SNR and wavelength shift, the FPC shows improvements of 89% and 63% compared to MDA and CCA, respectively. However, when $\Delta\lambda$=20 pm, because of the peak locking, the improvement introduced by the FPC compared to MDA reaches the 93% for precision and the 83% for accuracy. At the same time, compared to CCA, the precision decreases by 64% while the accuracy improves by 62%. This happens because the proposed FPC algorithm exhibits a less evident peak locking phenomenon compared to the MDA and CCA techniques. Figures 3 and 4 also show how the wavelength resolution affects the detection performances. The resolution has an attenuated influence on the FPC precision, which deteriorates only slightly when the resolution decreases from 10 to 35 pm, especially for SNR levels above 45 dB. This makes the selection of the spectral resolution quite flexible. The effect of the resolution on the accuracy is

#202834 - $15.00 USD Received 11 Dec 2013; revised 12 Feb 2014; accepted 16 Feb 2014; published 19 Mar 2014

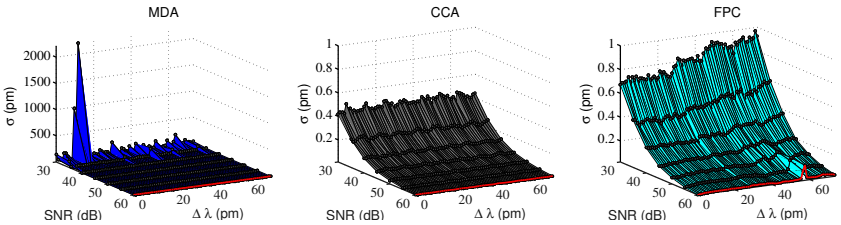

(a) Sample resolution $\delta\lambda = 10$ pm ($N = 61$)

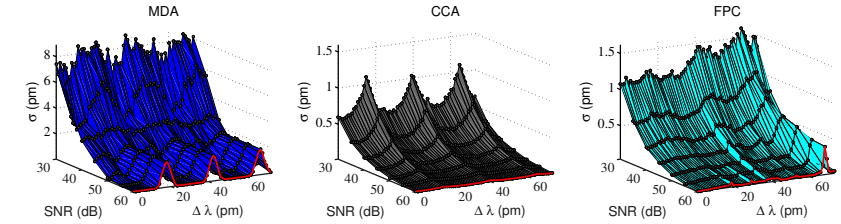

(b) Sample resolution $\delta\lambda = 25$ pm ($N = 25$)

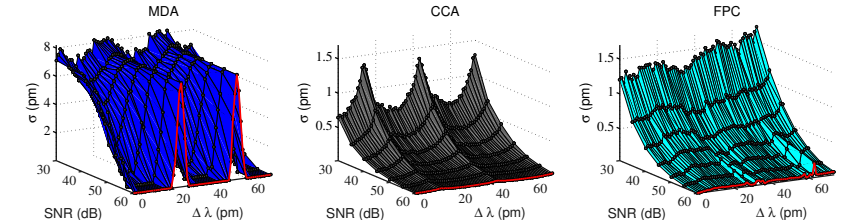

(c) Sample resolution $\delta\lambda = 30$ pm ($N = 21$)

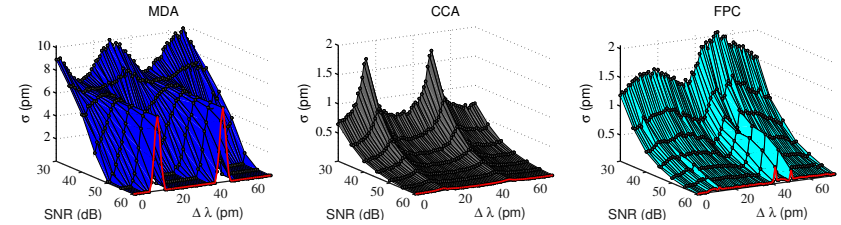

(d) Sample resolution $\delta\lambda = 35$ pm ($N = 18$)

Fig. 3. Precision of MDA, CCA and FPC algorithms for different wavelength resolutions. The MDA is used in conjunction with a 10 points quadratic interpolation around the maximum. The FPC is as precise as the CCA and considerably more precise than MDA. The peak locking effect is less evident for the FPC than for MDA and CCA.

more evident, however. The accuracy of the FPC can be up to 50 times worse going from $\delta\lambda$=10 pm to $\delta\lambda$=35 pm. Besides precision and accuracy, the computation time is another key factor for the evaluation of the performance of the proposed FPC algorithm. Table 1 reports the FPC computation performance in comparison with the MDA and CCA algorithms. To ease the comparison, all the values have been normalized using the execution time of the MDA algorithm as a reference. The analysis was performed with an $Intel\ \circledR\ Core^{TM}\ i7-3740QM\ CPU$ @2.70 GHz processor. It is evident that the FPC has the best performance, independently from the number of samples N used for the analysis. More specifically, the FPC is 5 to 6.35 times faster than the

#202834 - $15.00 USD Received 11 Dec 2013; revised 12 Feb 2014; accepted 16 Feb 2014; published 19 Mar 2014

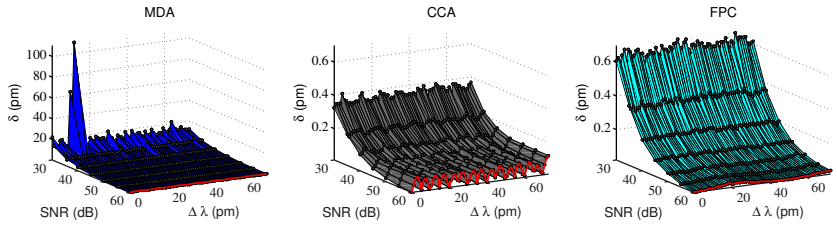

(a) Sample resolution $\delta\lambda = 10$ pm ($N = 61$)

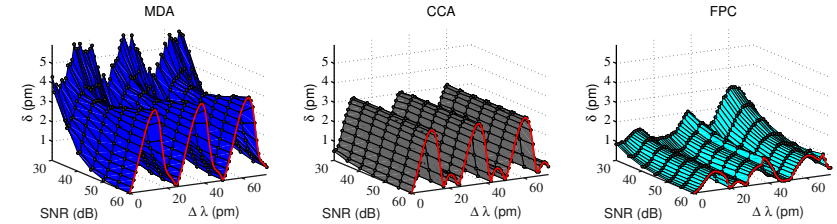

(b) Sample resolution $\delta\lambda = 25$ pm ($N = 25$)

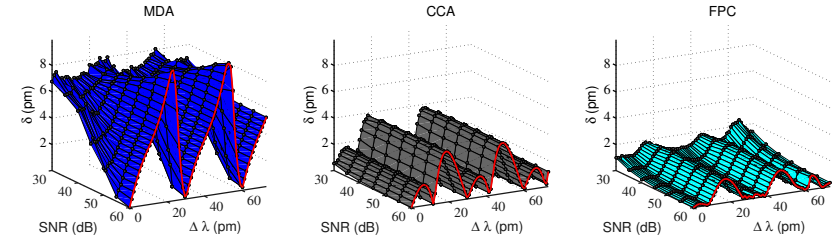

(c) Sample resolution $\delta\lambda = 30$ pm ($N = 21$)

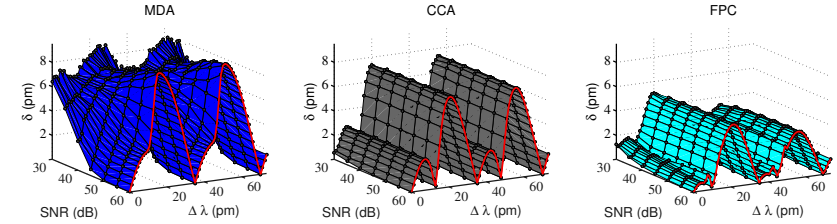

(d) Sample resolution $\delta\lambda = 35$ pm ($N = 18$)

Fig. 4. Accuracy of MDA, CCA and FPC algorithms for different wavelength resolutions. The FPC is generally more accurate than CCA and MDA and shows a less evident peak locking effect.

MDA and 30.15 to 50.18 times faster than the CCA.

For N=500, the time for a single phase correlation calculation is about 1 ms. From a practical point of view this means that, the proposed FPC algorithm would allow real time measurements at a scanning frequency of about 1 kHz. Tables 2 and 3 show the precision and accuracy of the peak detection algorithm when $\Delta\lambda$=0 and SNR=55 dB.

Although the reported values cannot be considered as absolute because of the previously explained peak locking effect, they provide a reference for comparing the performance of the three peak detection methods. Looking at Tables 1, 2 and 3 it is clear that the proposed FPC

#202834 - $15.00 USD Received 11 Dec 2013; revised 12 Feb 2014; accepted 16 Feb 2014; published 19 Mar 2014

Table 1. Normalized Time With Respect to MDA

N	MDA	CCA	FPC	CCA/FPC
61	1	8.03	0.16	50.18
500	1	7.33	0.18	40.72
1000	1	6.03	0.20	30.15

Table 2. Precision of the peak detection algorithm at $\Delta\lambda$=0 pm and SNR=55 dB

N	MDA (pm)	CCA (pm)	FPC (pm)
61	1.721	0.025	0.040
500	2.07	0.009	0.014
1000	1.549	0.005	0.009

Table 3. Accuracy of the peak detection algorithm at $\Delta\lambda$=0 pm and SNR=55 dB

N	MDA (pm)	CCA (pm)	FPC (pm)
61	1.539	0.021	0.035
500	2.632	0.008	0.011
1000	1.102	0.004	0.007

method represents a good trade-off between peak detection capabilities and computational requirements, yielding almost the same precision and accuracy of the CCA algorithm but with a computational effort lower than that required by a simple MDA algorithm.

4. Experiments and results

Experiments were carried out to validate the simulations and to demonstrate the effectiveness of the proposed FPC algorithm. The experimental setup is shown in Fig. 5. Three FBG sensors are glued on the lateral surface of a cylindrical steel bar and connected with a commercially available sm125 Bragg grating interrogator [24]. The wavelength range of the interrogator goes from 1510 to 1590 nm with a resolution of 5 pm. To better test the FPC capabilities, both type

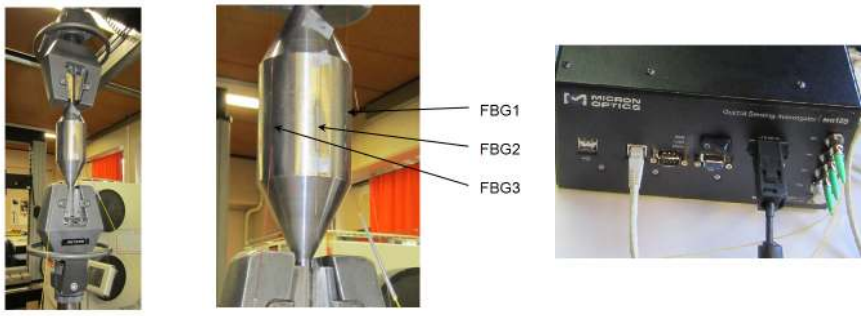

(a) (b) (c)

Fig. 5. Experimental setup: (a) steel test bar mounted on the stress testing machine; (b) zoom of the three FBG sensors glued on the steel bar; (c) interrogator.

I and type II gratings were adopted for the measurements. Type I gratings are associated with refractive index modulation occurring below the damage threshold of glass and they are char-

#202834 - $15.00 USD Received 11 Dec 2013; revised 12 Feb 2014; accepted 16 Feb 2014; published 19 Mar 2014

acterized by negligible losses in the reflected spectra. Type II gratings, instead, are written at high power and are associated with changes in the refractive index above the damage threshold of glass. Compared to type I, type II gratings are stable at much higher temperature (over 1000 °C), but they can suffer from significant scattering loss.

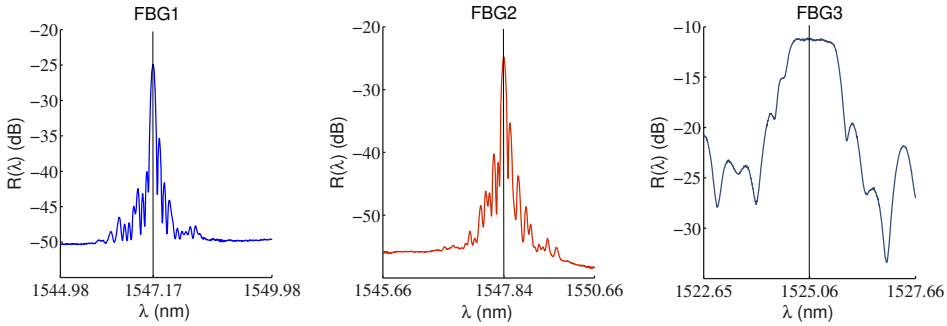

Fig. 6. FBGs reflectivities when no strain is applied. FBG1 and FBG2 are type I gratings while FBG3 is a type II grating. The peak region of FBG3 shows a plateau of about 0.8 nm, increasing the peak detection uncertainty.

Two of the FBG sensors that we used, FBG1 and FBG2, have a type I grating while the third sensor FBG3 has a type II grating. Figure 6 shows the reflected spectra of the three FBG sensors when no force is applied to the test bar. The Bragg wavelengths in this condition are 1547.17, 1547.84 and 1525.06 nm for FBG1, FBG2 and FBG3 respectively. The tensile test machine applies a strain rate of 100 $\mu\varepsilon/sec$. The FBGs reflected spectra are measured by the interrogator with a frequency of 2 Hz, stored and successively processed using the FPC, CCA and MDA algorithms. The wavelength shift of each FBG is computed using a wavelength window of 5 nm (N=1001) centered around the initial Bragg wavelength. Since at each time instant the exact wavelength shift is unknown, the precision of the algorithms is evaluated here as the standard deviation of the L_1 error between the measured data and their cubic fitting. Figures 7-9 report the computed wavelength shifts as function of time.

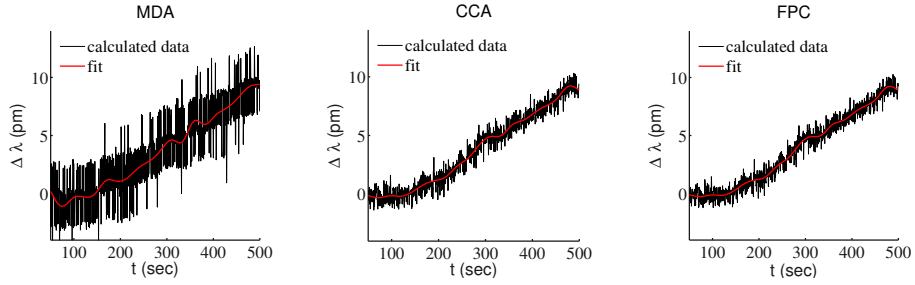

Fig. 7. Wavelength shift of FBG1 sensor computed with MDA, CCA and FPC. The precision σ of each algorithm is 1.882 pm (MDA), 0.597 pm (CCA) and 0.548 pm (FPC).

As expected, the proposed FPC algorithm shows the highest precisions of 0.548 pm, 0.587 and 1.543 pm on FBG1, FBG2 and FBG3 respectively. Compared to MDA and CCA, the FPC algorithm improves the resolution by 71% and 9% in FBG1, 69% and 3% in FBG2 and 99% and 53% in FBG3. The FPC performs quite well independently from the type of grating.
Comparing the type 1 gratings (Figs. 7 and 8) with the type 2 grating (Fig. 9) reveals a loss

#202834 - $15.00 USD Received 11 Dec 2013; revised 12 Feb 2014; accepted 16 Feb 2014; published 19 Mar 2014

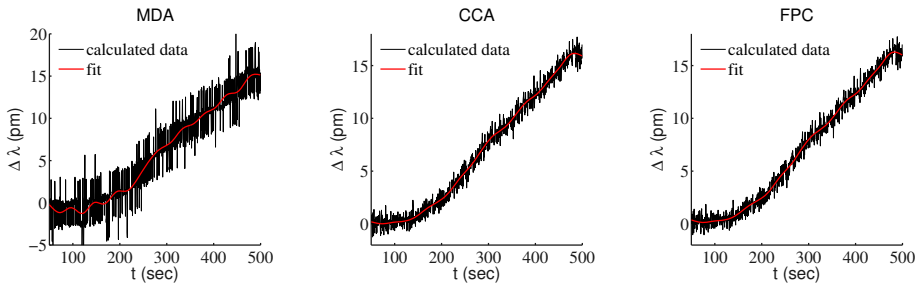

Fig. 8. Wavelength shift of FBG2 sensor computed with MDA, CCA and FPC. The precision σ of each algorithm is 1.865 pm (MDA), 0.599 pm (CCA) and 0.587 pm (FPC).

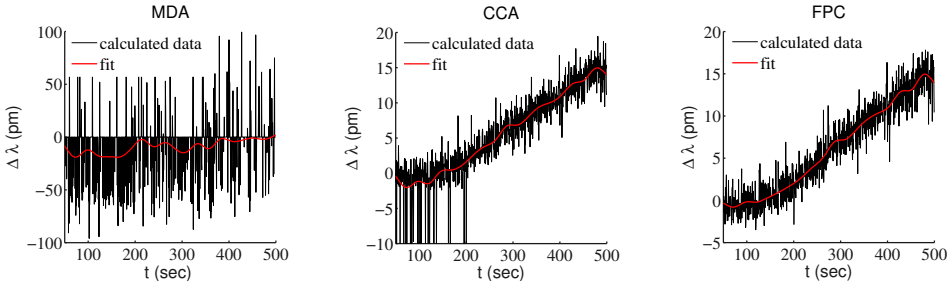

Fig. 9. Wavelength shift of FBG3 sensor computed with MDA, CCA and FPC. The precision σ of each algorithm is 451.25 pm (MDA), 2.23 pm (CCA) and 1.05 pm (FPC).

of precision of 49% for the FPC and of 74% and 99% respectively for the CCA and MDA. For FBG3, the extremely poor precision exhibited by the MDA algorithm is due to a combined effect of the shape of the reflected spectrum (FBG3 in Fig. 6) and the intrinsic nature of the peak searching algorithm. The FBG3 spectrum features a plateau of about 0.8 nm in the peak region, which complicates the detection of the maximum and makes it much more sensitive to noise fluctuations. On the contrary, the FPC and CCA perform better since they compute the wavelength shift without searching for the maximum. The FPC, in addition, presents lower precision variance of the CCA since it does not rely on subpixel interpolation to increase the precision. Figure 9 shows a high error level for CCA, which disappears after 200 seconds. This is a combined effect of sub-resolution interpolation, selected wavelength acquisition bandwidth and applied strain. For the first 200 seconds of measurements, the applied strain is so small that the cross-correlation vector is not symmetric and has its maximum value in the first position. In addition, the peak region is broad and flat, making therefore the interpolation routine less effective. After 200 seconds, the applied strain is enough high to move the peak value of the cross-correlation vector far from the first position. The cross-correlation acquire more symmetry and the peak region becomes sharper, allowing a better cubic interpolation. The effect of the wavelength bandwidth is shown in Fig. 10. Compared to Fig. 9, the wavelength bandwidth has been increased of 3 nm. In this case, for t$<$200 seconds, the CCA produces better results than in Fig. 9 since the augmented wavelength bandwidth yield to a sharper and narrower cross-correlation peak. Differently from CCA, the FPC algorithm is less influenced by the size of the wavelength window even though it performs better for lower wavelength bandwidth. According to the author, this is an additional positive feature of the FPC algorithm since a wavelength bandwidth reduction is often desirable to restrain the number of samples and to deal with multiple sensors at the same time.

#202834 - $15.00 USD Received 11 Dec 2013; revised 12 Feb 2014; accepted 16 Feb 2014; published 19 Mar 2014

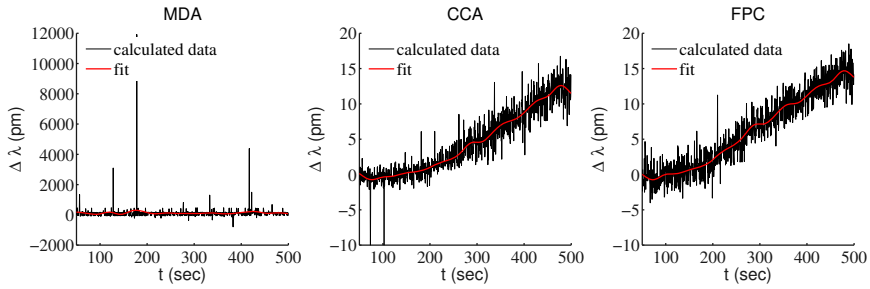

Fig. 10. Wavelength shift of FBG3 sensor computed with MDA, CCA and FPC using a wavelength bandwidth of 8 nm (N=1600). The precision σ of each algorithm is 455.45 pm (MDA), 1.51 pm (CCA) and 1.58 pm (FPC).

The effectiveness of the FPC method was also analyzed for different values of the wavelength resolution. Since the lowest resolution allowed by our interrogator was 5 pm, we artificially modified the resolution by processing sparse spectra obtained by leaving out samples from the original measurements. Figure 11 displays the evolution of the peak wavelength σ with respect to resolution. As the resolution step increases, the FPC continues to provide good sensing precision. Considering FBG1 and FBG2, the FPC peak wavelength σ first shows a slight increase, then the curves remain almost flat up to a resolution of 55 pm. The σ values are confined between 0.548 and 0.821 pm for FBG1 and between 0.587 and 0.891 pm for FBG2. The FPC precision is worse for FBG3, with values going from a minimum of 1.051 pm at 5 pm resolution, to a maximum 2.091 pm at a 50 pm resolution. Compared with CCA, the FPC precision is always better for FBG3. For FBG1 and FBG2 the FPC is more precise than CCA up to a resolution of 40 pm, while for values of resolution above this limit the cross correlation performs slightly better.

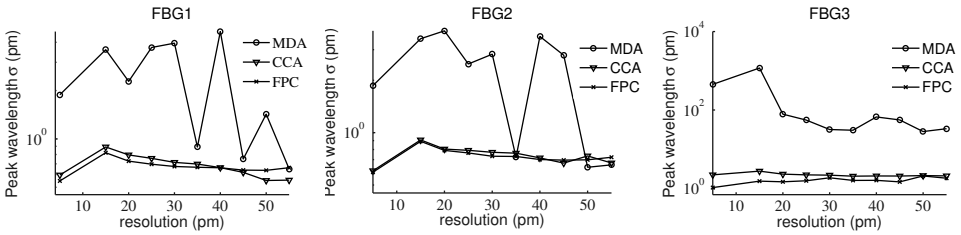

Fig. 11. Standard deviation σ of the calculated peak wavelength versus sample spectral resolution.

The MDA algorithm produces the worst results, especially for the type 2 grating sensor (FBG3). In this case, the peak wavelength σ tends to be lower as the resolution decreases from 5 to 35 pm and becomes almost stable for higher resolutions. When the resolution step increases, the frequency bandwidth spanned by the 10 points quadratic interpolation used by the MDA also increases, allowing for a better approximation of the peak region and making the algorithm more stable. Despite this improvement, the MDA precision never reaches the same level of CCA and FPC. At a 40 pm resolution, for example, the precision of the MDA algorithm is 3.575 pm for FBG1, 4.467 pm for FBG2 and 66.71 pm for FBG3, against the 0.661, 0.701

#202834 - $15.00 USD Received 11 Dec 2013; revised 12 Feb 2014; accepted 16 Feb 2014; published 19 Mar 2014

and 1.622 pm obtained by the FPC. This results suggest that, in contrast to the MDA, the FPC could operate in combination with low resolution interrogator systems while still guaranteeing a high sensing precision.

5. Conclusion

In this paper, we proposed a novel peak detection technique based on phase correlation. Using simulations and experiments we investigated the performances of the proposed FPC algorithm under different sample resolutions and SNR. We compared the FPC performances with the maximum detection algorithm (MDA) and with the cross-correlation algorithm (CCA). The FPC has the same order of measurements uncertainty as the cross-correlation algorithm but with a lower sensitivity to peak locking effect, especially at low SNR. Moreover, compared to MDA, the FPC is less influenced by wavelength resolution. Therefore, it allows using interrogator systems with lower wavelength resolution, with a consequent advantage not only it terms of acquisition speed but also in terms of cost of the device. The analyses of experimental measurements proved that the FPC is less sensitive to spectral shape and provides high precision also in the case of FBG with a type 2 grating. In terms of computational time, the FPC is one order of magnitude faster than CCA, with an execution speed of 1 ms when the number of spectral samples is set to 500. These characteristics make the FPC a suitable method for real time sensing applications and for future implementation in dynamic sensing systems.

Acknowledgments

This research has been performed in the framework of the SBO Project "Self Sensing Composites" funded by the Flemish Agency for Innovation by Science and Technology (IWT). The authors also acknowledge the Fund for Scientific Research - Flanders (FWO) and the COST TD1001 action OFSeSA.

#202834 - $15.00 USD Received 11 Dec 2013; revised 12 Feb 2014; accepted 16 Feb 2014; published 19 Mar 2014